Title

Sub-100nm, long tumor retention SN-38-loaded photonic micelles for tri-modal cancer therapy

Authors

Yang, Xixiao

Xue, Xiangdong

Luo, Yan

et al.

Publication Date

2017-09-01

DOI

10.1016/j.jconrel.2017.07.014

Peer reviewed

HHS Public Access

Author manuscript

J Control Release. Author manuscript; available in PMC 2018 September 10.

Published in final edited form as:

J Control Release. 2017 September 10; 261: 297–306. doi:10.1016/j.jconrel.2017.07.014.

Sub-100 nm, Long Tumor Retention SN-38-Loaded Photonic Micelles for Tri-modal Cancer Therapy

Xixiao Yang[a,b,1], **Xiangdong Xue**[a,1], **Yan Luo**[c], **Tzu-yin Lin**[d], **Hongyong Zhang**[d], **Diana Lac**[a], **Kai Xiao**[e], **Yixuan He**[a], **Bei Jia**[a], **Kit S. Lam**[a,d], and **Yuanpei Li**[a,*]

[a]Department of Biochemistry and Molecular Medicine, UC Davis Comprehensive Cancer Center, University of California Davis, Sacramento, CA 95817, USA

[b]Department of Pharmacy, Nanfang Hospital, Southern Medical University, Guangzhou 510515, PR China

[c]Department of Oncology, 153 Central Hospital, Zhengzhou 450042, PR China

[d]Department of Internal Medicine, Division of Hematology/Oncology, University of California Davis, Sacramento, CA 95817, USA

[e]National Chengdu Center for Safety Evaluation of Drugs, West China Hospital, Sichuan University, Chengdu, 610041, PR China

Abstract

The tumor penetration and accumulation of nanoparticle-based drug delivery systems are highly dependent on the particle size. Nanomedicines in the sub-100 nm range have been suggested by previous studies to have superior antitumor efficacy on various solid tumors. SN-38 is a very important and highly potent drug for several cancers including colon cancer. However, due to the ultra-flat aromatic structure of SN-38, it is typically very difficult to produce sub-100 nm, SN-38-encapsulated nanoparticles without modification of the chemical structure. Here, we report on the successful production of 20–30 nm, SN-38-encapsulated photonic micelles for effectively trimodal cancer therapy. Taking advantages of the supramolecular "**π -π**" stacking and hydrophobicity interaction between SN-38, and a unique class of photonic nanoporphyrin micelles (NPM), the extremely hydrophobic SN-38 was successfully encapsulated into NPM with significantly increased water solubility (up to 500 times). At equivalent dose of drug photosensitizer and light irradiation, combination therapy with SN-38-encapsulated nanoporphyrin micelles (SN-NPM) enhanced the *in vitro* antitumor activity by 78 and 350 times over single treatment with SN-38 and phototherapy alone, respectively. Due to the relatively small size, SN-NPM possessed superior long tumor retention time (> 5 days) and much higher accumulation in tumors than in normal organs, as shown by near-infrared fluorescence (NIRF) imaging. Furthermore, the trimodal therapy (photothermal-, photodynamic- and chemo-therapy) with SN-NPM demonstrated

*Address correspondence to Yuanpei Li (lypli@ucdavis.edu).

[1]These authors contributed equally.

dramatically enhanced *in vivo* antitumor efficacy over single treatment on nude mice bearing HT-29 colon cancer xenograft. Therefore, these sub-100 nm, SN-38-encapsulated photonic micelles show great promise for multimodal cancer therapy.

Graphical abstract

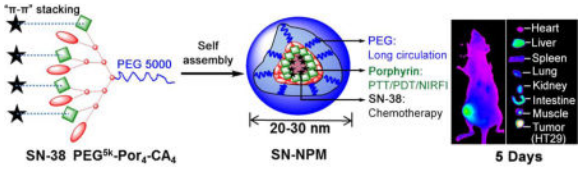

Keywords

Trimodal therapy; long tumor retention; drug delivery; "**π-π**" stacking; nanoporphyrin micelles

1. Introduction

Multimodal combination therapy that utilizes synergistic strategies to treat tumors has great potential to achieve enhanced treatment outcomes and minimize systemic toxicities[1–5]. Light-based therapeutic modalities such as photodynamic therapy (PDT) and photothermal therapy (PTT) hold great promise for cancer treatment[6–15]. PDT is a minimally invasive therapeutic modality by using reactive oxygen species (ROS) to trigger a cascade of molecular events that lead to cell death upon irradiation of photosensitizers with light. Unlike radiotherapy, the mechanism of cell killing by PDT is not dependent on DNA damage or cell cycle effects, and thus reducing the possibilities of therapy cross-resistance. PTT involves the administration of photosensitizers to generate significant local hyperthermia under light irradiation for the destruction of cancer cells or tissues[6–11,16–19], which does not require oxygen to interact with the target cells or tissues.

As both PDT and PTT have been proven to be effective treatment strategies for cancer, the approach of using nanoparticles to combine them into a single treatment modality may offer even better treatment efficacy[20]. There have been studies showing that PTT has synergistic effect with PDT and could further enhance the outcome of PDT by increasing local permeability of the sensitizers[7–10,16–17,19,21]. A few photosensitizer-inorganic nanoparticle complexes, such as chlorin e6 loaded graphene oxide and photosensitizers conjugated carbon nanotubes, silica-coated Pd/Ag nanoparticles and gold-based nanoparticles, have been developed for applications in PTT/PDT dual therapy[7–10,16–17,19,21–23]. However, to achieve dual PTT/PDT function, these nanoparticles were required to be activated under multiple-wavelength lasers (e.g. 675 nm and 808 nm), separately. Moreover, those inorganic nano-complexes were typically with less biocompatibility and ma y cause concerns of the long-term toxicity. Most recently, several organic nanoparticles, such as micelles, liposomes, and diketopyrrolopyrrole-triphenylamine nanoparticles contained near infrared (NIR) dye (e.g. IR780, IR820, Indocyanine green), were reported to possess excellent dual-modal PTT/PDT function[24–27].

Although dual-modal PTT/PDT appear to be very attractive conceptually, the light penetration limits its antitumor efficacy, and therefore make phototherapy could not be used to treat large tumor and metastasis, which is the major cause of cancer-related death. One promising approach is to combine phototherapy with chemotherapy, so that primary tumor and metastasis can both be adequately treated[28–29]. SN-38 (7-ethyl-10-hydroxycamptothecin) is a highly potent chemotherapy drug, and even effective in hypoxic tumor micro-environments[30–31]. It has been reported that SN-38 had synergistic effect with phototherapy[28–29]. SN-38 is the active metabolite of irinotecan hydrochloride (CPT-11), which is 100- to 1000-fold more cytotoxic than CPT-11[30,32–35]. The conversion rate from CPT-11 to SN-38 by carboxylesterases after administration is typically inefficient and usually yields only 2–8%[30,36–38]. Direct administration of SN-38 instead of CPT-11 would bypass the inefficient enzymatic activation, and therefore improve anticancer efficacy of this drug. However, SN-38 is virtually insoluble in all pharmaceutically acceptable solvents and is unable to be used directly to treat patients[37]. Furthermore, it is typically very challenging to physically encapsulate SN-38 into biocompatible nanoparticles such as polymeric micelles due to the unfavorable physicochemical properties of this drug, which are likely attributed to its moderate polarity and ultra-flat aromatic structure[37]. A few micelle-based drug delivery systems have been reported to solve the formulation problem of SN-38[28,30,37,39]. Several groups reported the production of SN38-encapsulated photonic nanoparticles such as chlorin-core star block copolymer micelles[28] and poly-(3,4-ethylenedioxythiophene):poly(4-styrenesulfonate) nanoparticles[40] with a particle size larger than 100 nm, attempting to use these nanoparticles to combine phototherapy with chemotherapy. However, these relatively large nanoparticles (>100nm) tend to high liver and spleen accumulation, resulting in non-specific clearance by the reticuloendothelial system (RES), obviating the enhanced permeability retention (EPR) effect for tumor targeting[39,41–43]. Smaller nanoparticles in the sub-100 nm range, such as 30 nm micelles, have been reported to be able to penetrate poorly permeable tumor, resulting in a better anti-tumor effect in animal models[39, 41–42].

We have previously demonstrated the biocompatible organic nanoporphyrin micelles (NPM) which could be activated to produce heat and ROS simultaneously at tumor site for dual-modal PTT/PDT with irradiation of a portable, single wavelength NIR light. In the present study, we describe the development of sub-100 nm SN-38 encapsulated photonic micelles for effectively tri-modal cancer therapy (PTT, PDT and chemotherapy). SN-38 was physically encapsulated in NPM by supramolecular "**π-π**" stacking and hydrophobicity interaction between SN-38 and porphyrins (Fig. 1). The chemical structure of SN-38 was not modified during the encapsulation, therefore avoiding the inefficient enzymatic activation step. To the best of knowledge, this is the first example of utilizing sub-100 nm SN-38 physically loaded photonic micelles for tri-modal cancer therapy. We hypothesized that these SN-38 loaded nanoporphyrin micelles (SN-NPM) may be able to improve the treatment outcomes of colon cancer in animal models.

2. Material and methods

2.1. Materials

Irinotecan hydrochloride (CPT-11) and SN-38 (7-thyl-10-hydroxy-camptothecin) were purchased from Sigma-Aldrich (St. Louis, MO). SensoLyte® Kit was obtained from AnaSpec, Inc. (Fremont, CA). Tetrazolium compound [3-(4, 5-dimethylthiazol-2-yl) -5-(3-carboxymethoxyphenyl)-2-(4-sulfophenyl)-2H-tetrazolium, MTS] and phenazine methosulfate (PMS) were purchased from Promega (Madison, WI). 3,3′-dihexadecyloxacarbocyanine perchlorate ($DiOC_6(3)$) was purchased from Thermo Fisher Scientific. All other chemicals and solvents were obtained from Sigma-Aldrich.

2.2. Preparation of SN-NPM

The building block of NPM, porphyrin-based telodendrimer, was synthesized via solution phase condensation reaction according to our published methods[20]. The SN-NPM were prepared by film hydration method as described in our previous studies[20]. Briefly, SN-38 and porphyrin-telodendrimer were dissolved in 1mL mixed chloroform and methanol (chloroform: methanol = 5:2, v/v) followed by sonication until the formation of a clear solution. The drug to telodendrimer ratios (D/T ratio=weight of SN-38/telodendrimer) were tested from 1:10 to 1:30. The resulting homogeneous solution was evaporated on rotavapor to obtain a homogeneous dry film. The film was then reconstituted in 1 mL phosphate buffered solution (PBS), followed by sonication for 20 min, allowing the film to be rehydrated to form SN-NPM. The micellar solution was filtered through a 0.22 μm cellulose acetate filter membrane to remove non-incorporated drug precipitations and big telodendrimer aggregates as well as sterilize the nanoparticles.

2.3. Characterization of SN-NPM

A Waters HPLC system equipped with a diode array UV detector was used to analyze the SN-38 that encapsulated in NPM. The mobile phase consisted of a mixture of water and acetonitrile (50:50, v/v%). C18 analytical column (150 mm 4.6 mm, 5 μm, Waters) was employed to separate the samples, and the flow speed was set to 1 mL/min, the whole eluting procedure lasted for 10 min. SN-38 was detected at 360 nm and quantitatively determined by an external calibration curve. The calibration curve was obtained using a series of drug/DMSO standard solutions with different concentrations. The SN-NPM were diluted with DMSO (SN-NPM solution/DMSO=1:9, v/v) to dissociate nanoparticles. The encapsulation efficiency (EE%) and loading content of SN-38 in NPM were calculated by using the following equations: EE%= [(SN-38 added - Free “unencapsulated SN-38”)/SN-38 added] *100, while the drug content (%) = [encapsulated SN-38/weight of SN-NPM] * 100.

The mean diameter and polydispersity of micelles were measured by dynamic light scattering (DLS) instruments (Microtrac), and data was analyzed by Microtrac FLEX Software 10.5.3. The concentration was kept at 1.0 mg/mL for DLS measurements. All measurements were performed at 25 °C. The morphology of the micelles was observed by TEM (Philips CM-120).

2.4. Stability of SN-NPM

SN-NPM were diluted to 50 μg/mL (SN-38 concentration) by PBS and 10% FBS (in PBS) respectively then stored at ambient temperature. The time-dependent size distributions were monitored by DLS to evaluate the stabilities of SN-NPM.

2.5. Accumulated drug release

SN-NPM solution was prepared to determine the accumulated drug release profile. The initial SN-38 concentration in SN-NPM was set as 100 μg/mL. SN-NPM was first loaded into dialysis cartridges (Pierce Chemical Inc.) with a MWCO of 3,500 Da, the cartridges were then submerged into 1,000 mL PBS at ambient temperature under moderate-speed stirring. The light-triggered drug release was conducted by introducing a 45 J/cm^2 laser exposure after 4 hrs dialysis. The SN-38 remained in the dialysis cartridge was drawn with a micro-syringe at various time points, and quantitatively measured by HPLC. Each value was reported as the means for each triplicate sample.

2.6. Cellular uptake study

The quantitative cellular uptake of SN-NPM by HT-29 cells was analyzed by flow cytometry. In time-dependent cellular uptake analysis, 3×10^5 HT-29 cells were incubated with SN-NPM (0.5 μg/mL SN-38 in 10 μg/mL NPM) at different time (5, 15, 60, 120, 300, 600, 1440 min) at 37 °C. For dose-dependent uptake experiments, 3×10^5 HT-29 cells were incubated with different concentrations (0, 2, 10, 20, 100, 200, 1000 μg/mL NPM in SN-NPM) of SN-NPM for 5 min. After the treatments, the cells were washed with cold PBS three times and re-suspended in PBS for the flow cytometry analysis using the FACScan (Becton Dickinson, San Jose, CA).

2.7. ROS production and cell death analysis

To evaluate the *in vitro* ROS production, HT-29 cells were treated with or without SN-NPM (0.5 μg/mL SN-38 in 10 μg/mL NPM) for 24 hours, prior to the 30 min 2′,7′-Dichlorofluorescin diacetate (DCF) incubation in 96 well plate. The medium was then washed off with PBS for three times, and replaced with fresh medium. The cells in each well were illuminated with NIR light and cell imaging was acquired under a fluorescence microscope (Olympus) by using Metamorph program. Next, to evaluate the SN-NPM caused mitochondria membrane potential ($\Delta\Psi m$) loss on HT-29 cells, we incubated the cells with 40 nM $DIOC_6(3)$ for 20 min, and exposed the cells under the illumination of 690 nm NIR light. Twenty-four hours later, cells were stained with propidium iodide (dead cells) and Hoechst 33342 (nucleus) for confocal microscopy analysis.

2.8. In vitro cytotoxicity

The HT-29 human colon cancer cell line was incubated in a humidified 5% CO_2 incubator at 37 °C in Dulbecco's Modified Eagle's Medium (DMEM) supplemented with 10% fetal bovine serum (FBS), 100 U/mL penicillin G, and 100 μg/mL streptomycin. HT-29 cells were first seeded into 96-well plates at a density of 10,000 cells per well and cultured. After 24 hrs, cells were incubated in medium containing different concentrations of SN-38, SN-NPM and the equivalent doses of empty NPM for 72 hrs, and washed off with PBS. The cells were

then exposed under NIR light for a given amount of time. Growth inhibition was measured after another 72 hrs by using MTS assay. CellTiter 96® Aqueous Cell Proliferation Reagent, which is composed of MTS and an electron coupling reagent PMS, was added to each well per the manufacturer's instructions. The cell viability was determined by measuring the absorbance at 490 nm with a microplate reader (SpectraMax M2, Molecular Devices, USA). Untreated cells served as a control. Results were shown as the average cell viability $[(OD_{treat}-OD_{blank})/(OD_{control}-OD_{blank})\times 100\%]$ of triplicate wells.

2.9. Apoptosis analysis

10 μg/mL of SN-NPM (contains 0.5 μg/mL SN-38) were incubated with HT-29 cell for 24 hours. Cells were washed with PBS and replaced with fresh cell culture medium. The SN-NPM treated cells were illuminated with NIR light for 60 s, and incubated for another 24 hrs. Before analyzed with flow cytometry, cells were stained with Annexin V/Propidium iodide (Biolegend) per manufactory's manual. The data was analyzed by flowjo.

2.10. Animal model

All animals were kept under pathogen-free conditions according to AAALAC guidelines and were allowed to acclimatize for at least 4 days prior to any experiments. All animal experiments were performed in compliance with institutional guidelines and according to protocol NO.07-13119 and NO.09-15584 approved by the Animal Use and Care Administrative Advisory Committee at the University of California, Davis. Male athymic nude mice (Nu/Nu strain, 6–8 weeks old) were purchased from the Harlan (Livermore, CA). HT-29 tumor was initially established by a subcutaneous injection of 10^6 cells in a 100 μL mixture of PBS and Matrigel (1:1, v/v). Tumor sizes and body weight were measured every 3 days for the duration of the experiment. Tumor volumes were calculated by the formula $(L\times W^2)/2$, where L is the longest, and W is the shortest in tumor diameters (mm).

2.11. Pharmacokinet ics analysis

Male Sprague–Dawley rats with jugular vein catheters were purchased from Harland (Indianapolis, IN, USA). 5 mg/kg SN-NPM (calculated by concentrations of SN-38) and CPT-11 were i. v. administrated into rats (n = 3 for each group). Whole blood samples (~100 μL) were collected via jugular vein catheter before dosing and at predetermined time points post-injection. Ten microliters of serum were further incubated with 90 microliters of DMSO to further break down the micelles and completely release SN-38. The kinetics of encapsulated SN-38 and free CPT-11 were measured through testing the fluorescence (excitation/emission, 330/460 nm). The values were plotted versus time after the subtraction of blood background.

2.12. Biodist ribution

PBS dispersed SN-NPM (10 mg/kg SN-38) was i.v. administrated into HT-29 tumor bearing nude mice via tail vein. At pre-determined time points (5 min, 16 hrs, 22 hrs, 72 hrs, 120 hrs) of post-injection, the mice were anesthetized by intraperitoneal injection of pentobarbital (60 mg/kg) prior to NIRF imaging. Mice were euthanized by CO_2 overdose at

22 hrs after injection. Tumors and major organs were excised and imaged. Mice and major organs were scanned on a Kodak imaging system (IS2000MM) by using the NIR channel.

2.13. Photothermal transduction of nanoporphyrins

The temperature of HT-29 tumor-bearing mice with or without injection of SN-NPM was monitored by a FLIR thermal camera after irradiation with NIR laser (690 nm) at 45 J/cm^2 and 90 J/cm^2 for 2 min, respectively.

2.14. Antitumor efficacy of SN-NPM

HT-29 tumors bearing mice were randomly divided into different groups (n=5) for the treatments with PBS, CPT-11 (in 10% glucose), NMP and SN-NPM. Treatments were started (designated as day 0) when HT-29 tumors reached a volume of 100–150 mm^3. Distinct formulations were administered via tail vein injections at multiple doses on day 0, 4, and 8 (10 mg/kg SN-38, 200 mg/kg NPM). After 24 hrs, tumors were exposed under the diode laser (λ =690 nm) with doses of 45 J/cm^2 or 90 J/cm^2 for 2 min. For humane reasons, animals were sacrificed when the implanted tumor volume reached 2000 mm^3, which was considered as the end point of survival data. Tumors and major organs were harvested 24 hrs after the light treatment from both PBS and SN-NPM treated groups for histopathology evaluation.

2.15. Histologic analysis

Histologic sections were collected from HT-29 tumor tissues and normal organs. After extirpation, tissues were fixed in 3.9% formalin in PBS (pH 7.4). The paraffin-embedded tumor and normal organs tissues were then sectioned to 4-μm thickness for hematoxylin and eosin (H&E) stain and microscopic evaluation.

2.16. Hematology and serum chemistry

Assessments on possible side effects were performed on mice of each group. At day 7 after the last dose, blood samples were collected for complete blood count (CBC) and liver (ALT, AST, Total Bilirubin) and kidney (BUN, Cre) functions. All assessments were performed at the Comparative Pathology Laboratory, University of California, Davis.

2.17. Statistical analysis

All statistic data were represented as mean ± standard deviation (s.d.). Statistical analysis was performed by Student's t-test for comparison of two relevant groups, and one-way analysis of variance (ANOVA) for multiple groups, followed by Newman–Keuls test if overall $p < 0.05$. $p<0.05$ was considered as significant difference.

3. Results & Discussion

3.1. Synthesis and characterization of SN-NPM

As illustrated in Fig. 1, SN-38 was physically encapsulated in NPM by supramolecular "**π - π**" stacking and hydrophobicity interaction between SN-38 and porphyrins. As shown in Table 1, the encapsulation efficiency (EE%) of SN-38 in NPM was around 85.12% when a

D/T ratio of 1:20 was employed, and the micelle solution was clear. When the D/T ratio reached 1:10, the EE% became lower (63.21%). The loading capacity of NPM for SN-38 was 5.45% (1.09 mg/mL), which increased the solubility of SN-38 in aqueous solution up to 500 times[38]. The morphology and size distribution of the nanoparticles were characterized by TEM and DLS, respectively. TEM showed that the empty NPM and SN-NPM (D/T ratio=1 20) were both in spherical morphology, and with a size of 20~30 nm (Fig. 2A, B). The size of empty NPM was approximately 25 nm in diameter as determined by DLS, which was consistent with the TEM result (Fig. 2C). After loading SN-38 into NPM with various D/T ratios, the size of micelles ranged from 20±4.5 nm to 68±5.9 nm as determined by DLS (Fig. 2C). It was reported that drug encapsulation efficiency is a crucial factor in the development of micelles or other drug delivery vesicles[44]. Therefore, the NPM, with efficient drug encapsulation and ideal size (20–30 nm) that was able to take full advantage of EPR effect for tumor targeting[39], was chosen as the drug carrier in this study. Specifically, SN-NPM with a D/T ratio of 120 possessed highest EE%, smaller particle size (23.21±8.23 nm) and lowest PDI (0.198) was selected among these three D/T ratios for the following *in vitro* and *in vivo* studies.

3.2. Stability evaluations of SN-NPM

The stability of SN-NPM was tested prior to the biological investigation. SN-NPM were incubated with or without the presence of FBS (10%) under ambient temperature. The size distributions were measured by DLS at different timepoints. As shown in Fig. S1, the size distributions of SN-NPM without FBS did not exhibit large size variations within a half month. When FBS was added, the size distributions of SN-NPM exhibited a very slight increment, from 21 nm to 22 nm, and kept stable in size. The stability indicated that SN-NPM could maintain high stability in presence of serum, and may be a benefit for long-time blood circulations.

3.3. Accumulated drug releasing behaviors of SN-NPM

The accumulated drug releasing behaviors of SN-NPM were evaluated. As shown in Fig. S2, the SN-NPM could keep stable in PBS solution, and didn’t show large amounts of payloads releasing pattern in 36 hrs, the accumulated drug releasing rate was below 20 %. On the contrary, the SN-NPM performed strong laser stimulus-responsive drug releasing behavior, since the presence of photosensitizer (porphyrin) could generate heat, and ma y further break the micelles. As shown in the drug releasing curve (Fig. S2), the drug releasing rate quickly reached to nearly 80% within 7 hrs after the laser treatment. The drug releasing profile indicated that the SN-NPM was stable under normal conditions, but exhibited controllable drug releasing behaviors under laser illumination.

3.4. Cellular uptake of SN-NPM

SN-NPM were incubated with HT-29 cells at 37 °C for pre-determined time, and the uptake by the cells was quantitatively measured by flow cytometry. As shown in Fig. S3, the cellular uptake of SN-NPM occurred quickly at 5 min and was in a time-dependent manner. Additionally, when incubated with different concentrations of SN-NPM for 5 minutes, cells had a dose-dependent cell uptake behavior (Fig. S4). These results provided a strong evidence of efficient cellular uptake of SN-NPM by HT-29 cells.

3.5. ROS production and cell death mechanisms

The ROS regulates many signal transduction pathways that control cell growth and redox status[45]. Excess ROS production could induce oxidative damage to many biomolecules and disrupt cellular integrity[46]. Accordingly, this study examined that the SN-NPM elevated ROS levels in HT-29 cells, and thus resulted in cell death following PDT treatments. We employed DCF as an indicator for intracellular ROS production. Cells were incubated with SN-NPM followed by light treatment, and showed strong diffused cytoplasmic green signals indicating massive ROS production (Fig. 3A). Conversely, cells incubated with PBS and PBS+L showed minimal fluorescence signal, indicating that either PBS or light alone did not produce ROS (Fig. 3B). ROS production stayed low when treated with SN-NPM until after illumination, suggesting that the ROS production was a light triggered process.

Moreover, we further characterized the effect of ROS production in the SN-NPM mediated photodynamic treatment in HT-29 human colon cancer cells. Consistent with the findings in Fig. 3, only the cells treated with SN-NPM associated ROS production upon illumination cause the loss of mitochondrial membrane potential ($DiOC_6(3)^{low}$) and cell death (PI^+) (Fig. 4). In other groups with low ROS production (Fig. 3), cells remained high mitochondrial membrane potential ($DiOC_6(3)^{high}$) and cell membrane integrity (PI-stained) (Fig. 4 and S5). In summary, human colon cancer cells could uptake SN-NPM and then ROS could be efficiently produced upon light treatment, and resulting in cellular damage and death. Without light treatment, lower ROS were produced and implied that we could well-controlled the light treatment areas that only treating the tumors but avoid undesirable toxicities.

3.6. Apoptosis of cells SN-NPM treated colon cancer cells

To further evaluate the mechanism of the decreased cell viability, we performed apoptosis analysis on HT-29 cells upon SN-NPM mediated light treatment. HT-29 cells were treated with PBS, SN-NPM or SN-NPM followed by light illumination. As shown in Fig. 5, the control (PBS plus light) and SN-NPM without light groups had around 2% and 6% of cells undergoing apoptosis. In contrast, there were 37.2% of cells in both early (26.4% annexin +/PI−) and late (10.8%, annexin+/PI+) apoptosis upon SP-NPM mediated photo-therapy These results suggested that SP-NPM mediated light treatment caused cell apoptosis and death.

3.7. In vitro photo-chemotherapeutic effects of SN-NPM against colon cancer cells

After characterized the properties and functions of SN-NPM, we intended to evaluate the anti-cancer efficacy on the HT-29 human colon cancer cell line. Cells were treated with SN-38, NPM, and SN-NPM followed with or without illumination as indicated. Cell viability was determined after 72 hrs post-illumination by MTS assay. As shown in Fig. 6A, NPM treated cells showed minimal toxicity without light activation. A dose-dependent loss of cell viabilities was shown in SN-38, NPM plus light and SN-NPM plus light treated groups. Importantly, the SN-NPM plus light groups exhibited strong cytotoxicity, which could be ascribe to the synergistic effects caused by SN-38 and NPM mediated light treatment. As shown in Fig. 6B, the combination index (CI) of all concentrations were showed strong synergistic effect (CI<0.3 indicates strong synergy). The IC_{50} values of

SN-38, NPM plus light, SN-NPM plus light in the HT-29 cell line were 267, 1193, and 3.4 ng/mL, respectively. This result indicated that at equivalent dose of drug, photosensitizer and light irradiation, combination therapy *via* SN-NPM enhanced the *in vitro* antitumor activity by 78 and 350 times over single treatment with SN-38 and phototherapy, respectively. The superior anti-cancer effects of SN-NPM ma y be contributed by the photochemical internalization (PCI) effect, a specific branch of PDT technology for the site-specific release of macromolecules or toxicants within cells based on the breakdown of endosomal/lysosomal membranes by photoactivation of photo-sensitizers. The micellar photosensitizing agent could be taken by cells via endocytosis and entrapped into the endosome/lysosome. After irradiation, PCI could disrupt the endocytic vehicles and enhance drug release to the cytosol[47]. Combination of photo-chemotherapeutic effects *via* SN-NPM showed great promising *in vitro* anti-colon cancer efficacy.

3.8. Pharmacokinetics of SN-NPM

The pharmacokinetic profile of SN-NPM was assessed in jugular vein catheterized rats, while an equal dose of CPT-11 was served as control. Fig 7 revealed SN-NPM exhibited 2 times higher C max and nearly 3 times higher area under the serum concentration time curve (AUC) to CPT-11. These results confirmed that NPM formulation offered SN-38 a longer circulation time allowing larger interaction window with cancers through EPR effects.

3.9. The biodistribution of SN-NPM in HT-29 bearing mice

By taking advantages of EPR effect, we previously showed that NPM could efficiently and effectively accumulate at several solid tumor types[20]. In this study, we also employed the intrinsic near-infrared fluorescence of SN-NPM to evaluate the biodistribution and tumor targeting properties in a mouse model bearing HT-29 colon cancer xenograft. After the establishment of tumors, SN-NPM were given intravenously and whole-body imaging was acquired at different time points. The accumulation of SN-NPM was firstly evident at 16 hrs gradually increased to peak at 22 hrs. The fluorescence signals remained high through 22–72 hrs post- injection and could still be well-detected even 120 hrs (=5 days) post-injection (Fig. 8), indicating relatively longer tumor retention of the SN-NPM.[48–51] Since the fluorescence appeared to peak at 22 hrs (Fig. S6), we sacrificed mice and harvested tumors and other major organs for *ex vivo* imaging. HT-29 xenograft tumor exhibited highest fluorescence signals comparing to other major organs, including liver, spleen, and lung (Fig. 8). These results showed that due to their unique size range (20~30 nm), these micelles were able to largely mitigate renal clearance (typically less than 10 nm) and RES (liver and spleen) retention (particles greater than 150 nm). Obvious NIRF signals indicated that SN-NPM could be specifically uptake by the colon cancers and be dissociated at the tumor sites, and thus allowing real-time NIRF detection. The SN-NPM could accumulate at tumor site at least 120 hrs post-injection, providing a very long-time window for the animals to receive light treatment. In the other words, this unique feature may offer more flexibility for both clinicians and patients for their treatment schedule.

3.10. In vivo heat production effect of SN-NPM

Besides ROS production and fluorescence emitting upon light activation, NPM could further generate significant heat for photothermal therapy[20]. We tested the SN-NPM mediated

photothermal effects on the mouse model bearing HT-29 colon cancer xenograft. After confirming the tumor accumulation of SN-NPM at 24 hrs (Fig 8), tumors were treated with 45 J/cm^2 and 90 J/cm^2 light at 690 nm for 2 minutes, respectively. The tumor temperature was monitored with a near-infrared thermal camera in real-time. The tumor temperature d id not change much in the PBS control group even treated with a high dose of light (90 J/cm^2). On the contrary, we showed a light dose-dependent tumor temperature increase in the SN-NPM treated mice. Specifically, a low dose of light (45 J/cm^2) treatment could cause ~10°C tumor temperature increase, while high dose of light (90 J/cm^2) triggered even more obvious heat escalation up and increase tumor temperature 19.1 °C(ΔT). The photothermal effects of SN-NPM (both in lo w and high light dose) were sufficient enough to cause irreversible damage on tumor cells[20]. The rapid temperature increase suggested SN-NPM as photothermal agents that could be used for selective photothermal therapy to induce cancer cell death via hyperthermia attained[52].

3.11. In vivo anti-tumor effects of SN-NPM mediated tri-modality therapy

The promising *in vitro* efficacy results urged us to explore the anti-tumor efficiency of SN-NPM in xenograft mouse model. HT-29 human colon cancer xenografts were established in nude mice; the treatments were then initiated when the tumor volume reached 100-150 mm^3. Light treatment was applied after 24 hrs of the i. v. administration. Mice were closely monitored for clinical signs of toxicity, body weights and tumor size. We activated NPM with two doses (45 and 90 J/cm^2) of 690 nm NIR light. Both CPT-11 (10 mg/kg) and NPM +45 J/cm^2 light showed slight tumor growth delay, while NPM+90 J/cm^2 exhibited moderate tumor growth inhibition (Fig. 10A and Table 2). Additionally, SN-NPM+45 J/cm^2 and SN-NPM+90 J/cm^2 treated groups achieve 71.96% and 84.86% of tumor growth inhibition (Table 2). Overall, SN-NPM+45 J/cm^2 and SN-NPM+90 J/cm^2 treated mice had stable tumor development tendency (no tumor size changes) or even partial remission (tumor size decreased), at the first 24 days of treatments (Fig. 10A). Some mice with SN-NPM mediated trimodal therapy even achieved initial complete remission with no palpable tumors. Although there were no significance differences in survival times between the most treated groups (ranging from 25 to 28 days), SN-NPM+90 J/cm^2 treated groups had significantly longer survival time (35 days, $p<0.05$) (Fig. 10B). Compared to PBS control group, SN-NPM treatment followed by 90 J/cm^2 light treatment caused massive tumor cell and microenvironment destruction (Fig. 11). The tumor cells shirked and nucleus became pyknotic and fragmented eventually resulting in cell death (Fig. 11). In summary, SN-NPM mediated trimodal therapy significantly inhibited tumor growth and prolonged survival time comparing to CPT-11, NPM/light treatment or PBS control groups, and thus a synergistic inhibitory effect of SN-NPM on colon cancer growth was demonstrated (Fig. 10A & B).

3.12. In vivo toxicity evaluations

Moreover, there was no significant systemic toxicity observed in the NPM or SN-NPM+ light treated groups evidenced by comparing the body weight changes with the PBS control group. However, CPT-11 treated mice exhibited slight retarded body weight increase indicating possible systemic toxicity (Fig. 10C). The complete blood count (CBC) and biochemistry studies (including hepatic and renal function panels) were performed at 7 days after the last dose in the same set of animals for systemic toxicity evaluations. There were no

significant differences in WBC, RBC, and platelet counts between the treated groups (CPT −11, NPM+90 J/cm^2, and SN-NPM+90 J/cm^2) and PBS control group (Table S1). All liver enzymes (ALT/AST), total bilirubin, and renal biomarkers (BUN and creatinine) were within normal limits (Table S2). In the SN-NPM treated animals, there was no significant pathological change in major organs, including those with rapid turnover rates, such as small intestine and livers (Fig. S7). Therefore, we concluded that SN-NPM can decrease the overall toxicity of CPT-11 based on the results on overall body weight change. SN-NPM exhibited superior safety profile and may facilitate its translation into a clinical setting.

4. Conclusions

In this study, the highly potent drug SN-38 was successfully encapsulated into nanoporphyrin micelles without modifying its chemical structure, leading to ~500 times solubility increments of this hydrophobic drug in aqueous solution. The nanoporphyrin micelles exhibited high drug encapsulation efficiency with an ideal size, which is suitable for tumor targeted drug delivery. SN-NPM exhibited significantly higher accumulation in tumor than that in normal organs, and possessed superior long retention time at the tumor site (> 5 days). SN-NPM not only served as a nano-formulated photosensitizer for PTT and PDT, but also acted a highly potent chemotherapeutic agent for effective chemotherapy. The triple modality therapy (PTT, PDT and chemotherapy) of SN-NPM significantly enhanced the *in vitro* antitumor activity over single treatment against HT-29 colon cancer cells. *In vivo* antitumor efficacy data clearly established that the micellar SN-38 formulation was therapeutically more effective than free CPT-11 in HT-29 human colon cancer xenograft model. Furthermore, the most significant improvement in tumor response was achieved by the tri-modality therapy group of SN-NPM. SN-NPM has the great potential to integrate PTT/PDT/chemotherapy with synergistic effects for effective cancer treatment.

Supplementary Material

Refer to Web version on PubMed Central for supplementary material.

Acknowledgments

The authors thank the financial support from NIH/NCI (R01CA199668 & 3R01CA115483), NIH/NIBIB (5R01EB012569), NIH/NICHD (1R01HD086195) and DoD PRMRP Award (W81XWH-13-1-0490).

Appendix A. Supplementary data

Supplementary data to this article can be found online at http://dx.doi.org/10.1016/j.jconrel.xxx

References

1. Lee DE, Koo H, Sun IC, Ryu JH, Kim K, Kwon IC. Multifunctional nanoparticles for multimodal imaging and theragnosis. Chem Soc Rev. 2012; 41(7):2656–72. [PubMed: 22189429]
2. Cho K, Wang X, Nie S, Chen ZG, Shin DM. Therapeutic nanoparticles for drug delivery in cancer. Clin Cancer Res. 2008; 14(5):1310–6. [PubMed: 18316549]

3. Mao F, Wen L, Sun C, Zhang S, Wang G, Zeng J, Wang Y, Ma J, Gao M, Li Z. Ultrasmall Biocompatible Bi2Se3Nanodots for Multimodal Imaging-Guided Synergistic Radiophotothermal Therapy against Cancer. ACS nano. 2016; 10(12):11145–11155. [PubMed: 28024338]

4. Duan S, Yang Y, Zhang C, Zhao N, Xu FJ. NIR-Responsive Polycationic Gatekeeper-Cloaked Hetero-Nanoparticles for Multimodal Imaging-Guided Triple-Combination Therapy of Cancer. Small. 2016

5. Zhang S, Sun C, Zeng J, Sun Q, Wang G, Wang Y, Wu Y, Dou S, Gao M, Li Z. Ambient Aqueous Synthesis of UltrasmallPEGylatedCu2-x Se Nanoparticles as a Multifunctional Theranostic Agent for Multimodal Imaging Guided Photothermal Therapy of Cancer. Adv Mater. 2016; 28(40):8927–8936. [PubMed: 27560922]

6. Agostinis P, Berg K, Cengel KA, Foster TH, Girotti AW, Gollnick SO, Hahn SM, Hamblin MR, Juzeniene A, Kessel D, Korbelik M, Moan J, Mroz P, Nowis D, Piette J, Wilson BC, Golab J. Photodynamic therapy of cancer: an update. CA Cancer J Clin. 2011; 61(4):250–81. [PubMed: 21617154]

7. Jin CS, Lovell JF, Chen J, Zheng G. Ablation of hypoxic tumors with dose-equivalent photothermal, but not photodynamic, therapy using a nanostructured porphyrin assembly. ACS nano. 2013; 7(3): 2541–50. [PubMed: 23394589]

8. Wang J, Zhu G, You M, Song E, Shukoor MI, Zhang K, Altman MB, Chen Y, Zhu Z, Huang CZ, Tan W. Assembly of aptamer switch probes and photosensitizer on gold nanorods for targeted photothermal and photodynamic cancer therapy. ACS nano. 2012; 6(6):5070–7. [PubMed: 22631052]

9. Kuo WS, Chang YT, Cho KC, Chiu KC, Lien CH, Yeh CS, Chen SJ. Gold nanomaterials conjugated with indocyanine green for dual-modality photodynamic and photothermal therapy. Biomaterials. 2012; 33(11):3270–8. [PubMed: 22289264]

10. Jang B, Park JY, Tung CH, Kim IH, Choi Y. Gold nanorod-photosensitizer complex for near-infrared fluorescence imaging and photodynamic/photothermal therapy in vivo. ACS nano. 2011; 5(2):1086–94. [PubMed: 21244012]

11. Demberelnyamba D, Ariunaa M, Shim YK. Newly synthesized water soluble cholinium-purpurin photosensitizers and their stabilized gold nanoparticles as promising anticancer agents. Int J MolSci. 2008; 9(5):864–71.

12. von Maltzahn G, Park JH, Agrawal A, Bandaru NK, Das SK, Sailor MJ, Bhatia SN. Computationally guided photothermal tumor therapy using long-circulating gold nanorod antennas. Cancer research. 2009; 69(9):3892–900. [PubMed: 19366797]

13. O'Neal DP, Hirsch LR, Halas NJ, Payne JD, West JL. Photo-thermal tumor ablation in mice using near infrared-absorbing nanoparticles. Cancer letters. 2004; 209(2):171–6. [PubMed: 15159019]

14. Bardhan R, Lal S, Joshi A, Halas NJ. Theranosticnanoshells: from probe design to imaging and treatment of cancer. AccChem Res. 2011; 44(10):936–46.

15. Moore CM, Pendse D, Emberton M. Photodynamic therapy for prostate cancer–a review of current status and future promise. Nature clinical practice Urology. 2009; 6(1):18–30.

16. Wang J, You M, Zhu G, Shukoor MI, Chen Z, Zhao Z, Altman MB, Yuan Q, Zhu Z, Chen Y, Huang CZ, Tan W. Photosensitizer-Gold Nanorod Composite for Targeted Multimodal Therapy. Small. 2013

17. Liao X, Zhang X. Preparation, characterization and cytotoxicity of carbon nanotube-chitosan-phycocyanin complex. Nanotechnology. 2012; 23(3):035101. [PubMed: 22173212]

18. Camerin M, Rello-Varona S, Villanueva A, Rodgers MA, Jori G. Metallo-naphthalocyanines as photothermalsensitisers for experimental tumours: in vitro and in vivo studies. Lasers Surg Med. 2009; 41(9):665–73. [PubMed: 19790243]

19. Kah JC, Wan RC, Wong KY, Mhaisalkar S, Sheppard CJ, Olivo M. Combinatorial treatment of photothermal therapy using gold nanoshells with conventional photodynamic therapy to improve treatment efficacy: an in vitro study. Lasers Surg Med. 2008; 40(8):584–9. [PubMed: 18798290]

20. Li Y, Lin TY, Luo Y, Liu Q, Xiao W, Guo W, Lac D, Zhang H, Feng C, Wachsmann-Hogiu S, Walton JH, Cherry SR, Rowland DJ, Kukis D, Pan C, Lam KS. A smart and versatile theranosticnanomedicine platform based on nanoporphyrin. Nature communications. 2014; 5:4712.

21. Tian B, Wang C, Zhang S, Feng L, Liu Z. Photothermally enhanced photodynamic therapy delivered by nano-graphene oxide. ACS nano. 2011; 5(9):7000–9. [PubMed: 21815655]
22. You Q, Sun Q, Wang J, Tan X, Pang X, Liu L, Yu M, Tan F, Li N. A single -light triggered and dual-imaging guided multifunctional platform for combined photothermal and photodynamic therapy based on TD-controlled and ICG-loaded CuS@mSiO2. Nanoscale. 2017
23. Liu J, Liu K, Feng L, Liu Z, Xu L. Comparison of nanomedicine-based chemotherapy, photodynamic therapy and photothermal therapy using reduced graphene oxide for the model system. Biomaterials science. 2017; 5(2):331–340. [PubMed: 27935610]
24. Wang K, Zhang Y, Wang J, Yuan A, Sun M, Wu J, Hu Y. Self-assembled IR780-loaded transferrin nanoparticles as an imaging, targeting and PDT/PTT agent for cancer therapy. Scientific reports. 2016; 6:27421. [PubMed: 27263444]
25. Yan F, Wu H, Liu H, Deng Z, Duan W, Liu X, Zheng H. Molecular imaging-guided photothermal/photodynamic therapy against tumor by iRGD-modified indocyanine green nanoparticles. J Control Release. 2016; 224:217–28. [PubMed: 26739551]
26. Li W, Peng J, Tan L, Wu J, Shi K, Qu Y, Wei X, Qian Z. Mild photothermal therapy/photodynamic therapy/chemotherapy of breast cancer by Lyp-1 modified Docetaxel/IR820 Co-loaded micelles. Biomaterials. 2016; 106:119–33. [PubMed: 27561883]
27. Cai Y, Liang P, Tang Q, Yang X, Si W, Huang W, Zhang Q, Dong X. Diketopyrrolopyrrole-Triphenylamine Organic Nanoparticles as Multifunctional Reagents for Photoacoustic Imaging-Guided Photodynamic/Photothermal Synergistic Tumor Therapy. ACS nano. 2017; 11(1):1054–1063. [PubMed: 28033465]
28. Peng CL, Lai PS, Lin FH, Yueh-Hsiu Wu S, Shieh MJ. Dual chemotherapy and photodynamic therapy in an HT-29 human colon cancer xenograft model using SN-38-loaded chlorin-core star block copolymer micelles. Biomaterials. 2009; 30(21):3614–25. [PubMed: 19395020]
29. Huang HC, Mallidi S, Liu J, Chiang CT, Mai Z, Goldschmidt R, Ebrahim-Zadeh N, Rizvi I, Hasan T. Photodynamic Therapy Synergizes with Irinotecan to Overcome Compensatory Mechanisms and Improve Treatment Outcomes in Pancreatic Cancer. Cancer research. 2016; 76(5):1066–77. [PubMed: 26719532]
30. Bala V, Rao S, Boyd BJ, Prestidge CA. Prodrug and nanomedicine approaches for the delivery of the camptothecin analogue SN38. Journal of controlled release: official journal of the Controlled Release Society. 2013; 172(1):48–61. [PubMed: 23928356]
31. Murono K, Tsuno NH, Kawai K, Sasaki K, Hongo K, Kaneko M, Hiyoshi M, Tada N, Nirei T, Sunami E, Takahashi K, Kitayama J. SN-38 overcomes chemoresistance of colorectal cancer cells induced by hypoxia, through HIF1 alpha. Anticancer Res. 2012; 32(3):865–72. [PubMed: 22399605]
32. England RM, Hare JI, Barnes J, Wilson J, Smith A, Strittmatter N, Kemmitt PD, Waring MJ, Barry ST, Alexander C, Ashford MB. Tumour regression and improved gastrointestinal tolerability from controlled release of SN-38 from novel polyoxazoline-modified dendrimers. Journal of controlled release: official journal of the Controlled Release Society. 2017; 247:73–85. [PubMed: 28043863]
33. Guo Q, Luo P, Luo Y, Du F, Lu W, Liu S, Huang J, Yu J. Fabrication of biodegradable micelles with sheddable poly(ethylene glycol) shells as the carrier of 7-ethyl-10-hydroxy-camptothecin. Colloids and surfaces B, Biointerfaces. 2012; 100:138–45. [PubMed: 22766290]
34. Ebrahimnejad P, Dinarvand R, Sajadi A, Jaafari MR, Nomani AR, Azizi E, Rad-Malekshahi M, Atyabi F. Preparation and in vitro evaluation of actively targetable nanoparticles for SN-38 delivery against HT-29 cell lines. Nanomedicine : nanotechnology, biology, and medicine. 2010; 6(3):478–85.
35. Gu Q, Xing JZ, Huang M, He C, Chen J. SN-38 loaded polymeric micelles to enhance cancer therapy. Nanotechnology. 2012; 23(20):205101. [PubMed: 22543761]
36. Liu Y, Piao H, Gao Y, Xu C, Tian Y, Wang L, Liu J, Tang B, Zou M, Cheng G. Comparison of two self-assembled macromolecular prodrug micelles with different conjugate positions of SN38 for enhancing antitumor activity. Int J Nanomedicine. 2015; 10:2295–311. [PubMed: 25848251]
37. Xu G, Shi C, Guo D, Wang L, Ling Y, Han X, Luo J. Functional-segregated coumarin-containing telodendrimernanocarriers for efficient delivery of SN-38 for colon cancer treatment. Actabiomaterialia. 2015; 21:85–98.

38. Wang H, Xie H, Wu J, Wei X, Zhou L, Xu X, Zheng S. Structure-based rational design of prodrugs to enable their combination with polymeric nanoparticle delivery platforms for enhanced antitumor efficacy. AngewChemInt Ed Engl. 2014; 53(43):11532–7.

39. Cabral H, Matsumoto Y, Mizuno K, Chen Q, Murakami M, Kimura M, Terada Y, Kano MR, Miyazono K, Uesaka M, Nishiyama N, Kataoka K. Accumulation of sub-100 nm polymeric micelles in poorly permeable tumours depends on size. Nature nanotechnology. 2011; 6(12):815–23.

40. Gong H, Cheng L, Xiang J, Xu H, Feng L, Shi X, Liu Z. Near-Infrared Absorbing Polymeric Nanoparticles as a Versatile Drug Carrier for Cancer Combination Therapy. Advanced Functional Materials. 2013; 23(48):6059–6067.

41. Luo J, Xiao K, Li Y, Lee JS, Shi L, Tan YH, Xing L, Holland Cheng R, Liu GY, Lam KS. Well-defined, size-tunable, multifunctional micelles for efficient paclitaxel delivery for cancer treatment. BioconjugChem. 2010; 21(7):1216–24.

42. Chauhan VP, Stylianopoulos T, Martin JD, Popovic Z, Chen O, Kamoun WS, Bawendi MG, Fukumura D, Jain RK. Normalization of tumour blood vessels improves the delivery of nanomedicines in a size-dependent manner. Nat Nanotechnol. 2012; 7(6):383–8. [PubMed: 22484912]

43. Wang J, Mao W, Lock LL, Tang J, Sui M, Sun W, Cui H, Xu D, Shen Y. The Role of Micelle Size in Tumor Accumulation, Penetration, and Treatment. ACS nano. 2015; 9(7):7195–206. [PubMed: 26149286]

44. Li Y, Xiao K, Luo J, Lee J, Pan S, Lam KS. A novel size-tunable nanocarrier system for targeted anticancer drug delivery. Journal of Controlled Release. 2010; 144(3):314–23. [PubMed: 20211210]

45. Liao ZX, Li YC, Lu HM, Sung HW. A genetically-encoded KillerRed protein as an intrinsically generated photosensitizer for photodynamic therapy. Biomaterials. 2014; 35(1):500–8. [PubMed: 24112805]

46. Hwang H, Biswas R, Chung PS, Ahn JC. Modulation of EGFR and ROS induced cytochromec release by combination of photodynamic therapy and carboplatin in human cultured head and neck cancer cells and tumor xenograft in nude mice. Journal of photochemistry and photobiology B, Biology. 2013; 128:70–7.

47. Lai PS, Lou PJ, Peng CL, Pai CL, Yen WN, Huang MY, Young TH, Shieh MJ. Doxorubicin delivery by polyamidoaminedendrimer conjugation and photochemical internalization for cancer therapy. J Control Release. 2007; 122(1):39–46. [PubMed: 17628166]

48. Feng Q, Yu M-Z, Wang J-C, Hou W-J, Gao L-Y, Ma X-F, Pei X-W, Niu Y-J, Liu X-Y, Qiu C, Pang W-H, Du L-L, Zhang Q. Synergistic inhibition of breast cancer by co-delivery of VEGFsiRNA and paclitaxel via vapreotide-modified core–shell nanoparticles. Biomaterials. 2014; 35(18):5028–5038. [PubMed: 24680191]

49. Yu Q, Liu Y, Cao C, Le F, Qin X, Sun D, Liu J. The use of pH-sensitive functional selenium nanoparticles shows enhanced in vivo VEGF-siRNA silencing and fluorescence imaging. Nanoscale. 2014; 6(15):9279–9292. [PubMed: 24986368]

50. Li J, Liu J, Wei C-W, Liu B, O'Donnell M, Gao X. Emerging applications of conjugated polymers in molecular imaging. Physical Chemistry Chemical Physics. 2013; 15(40):17006–17015. [PubMed: 23860904]

51. Kim J-H, Kim Y-S, Park K, Lee S, Nam HY, Min KH, Jo HG, Park JH, Choi K, Jeong SY, Park R-W, Kim I-S, Kim K, Kwon IC. Antitumor efficacy of cisplatin-loaded glycol chitosan nanoparticles in tumor-bearing mice. Journal of Controlled Release. 2008; 127(1):41–49. [PubMed: 18234388]

52. Ghosh S, Dutta S, Gomes E, Carroll D, D'Agostino R Jr, Olson J, Guthold M, Gmeiner WH. Increased heating efficiency and selective thermal ablation of malignant tissue with DNA-encased multiwalled carbon nanotubes. ACS nano. 2009; 3(9):2667–73. [PubMed: 19655728]

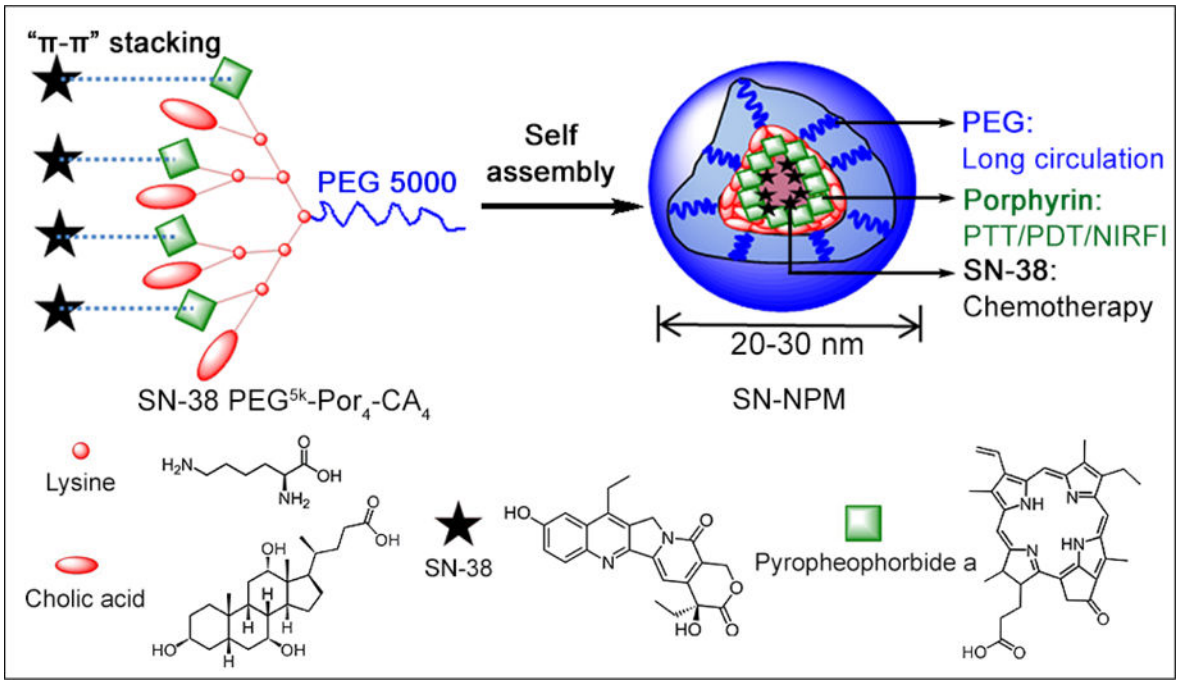

Fig. 1.

The schematic illustration of porphyrin-based telodendrimer $(PEG^{5k}\text{-}Por_4\text{-}CA_4)^{20}$ and the resulting multifunctional SN-38-encapsulated nanoporphyrin micelles (SN-NPM).

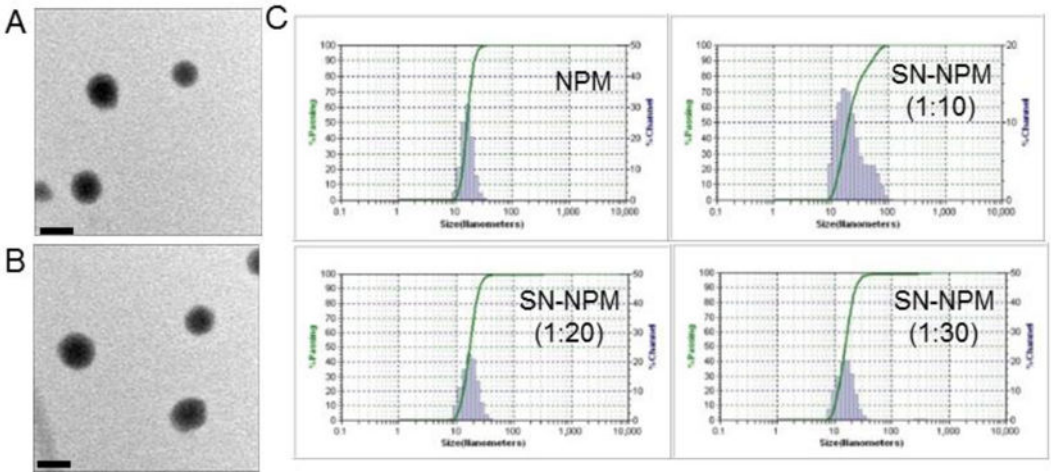

Fig. 2. The particle size and morphology of SN-NPM

The morphology of the as-prepared A) NPM and B) SN-NPM were determined by TEM (scale bar=20nm). C) Size distributions of NPM and SN-NPM with D/T ratios ranging from 1:10 to 1:30.

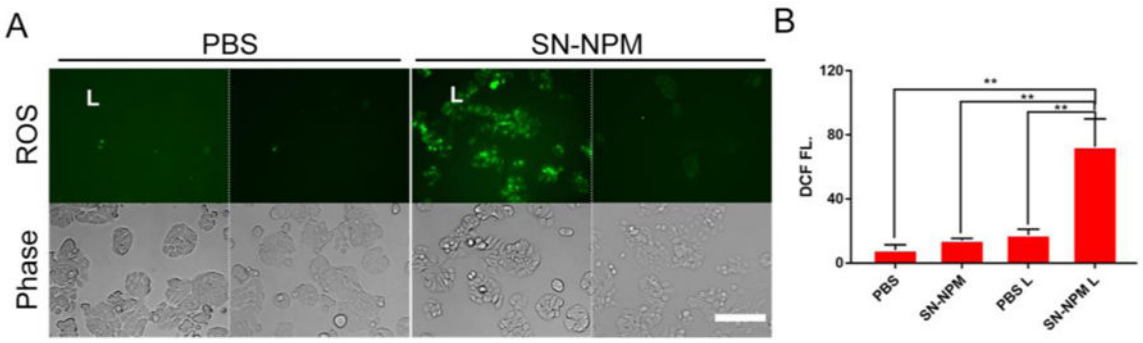

Fig. 3.

Intracellular ROS production in colon cancer cell line upon SN-NPM and light activation. A) CLSM images of ROS production on SN-NPM treated HT-29 cells B) Quantitative analysis of ROS production. The quantitative analysis was processed by ImageJ. Intracellular ROS production was monitored with 1 μM of DCF for 30 min. L: light treatment. Images were acquired by fluorescence microscope. Phase images were taken to show the cell outlines. (Scale bar=100 μm)

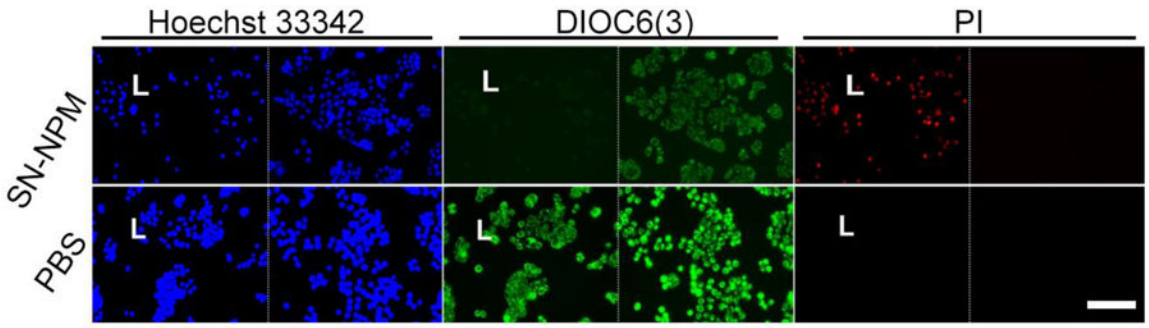

Fig. 4. The changes of mitochondria membrane potential and membrane integrity of HT-29 human colon cancer cells upon SN-NPM mediated light treatment

Cells were incubated with SN-NPM (0.5 μg/mL SN-38 in 10 μg/mL NPM) or PBS for 24 hrs in 96-well black-wall plate, and treated with or without light. Mitochondria membrane potential and cell membrane integrity were stained with 40 nM of $DiOC_6(3)$ (Green, $\Delta\Psi m$) and propridium iodide (PI, Red) at 24 hrs later post-light treatment, respectively. Nucleus was counterstained with Hoechst 33342. (L, light treatment; PI, propridium iodide; the sacle bar is 100 μm).

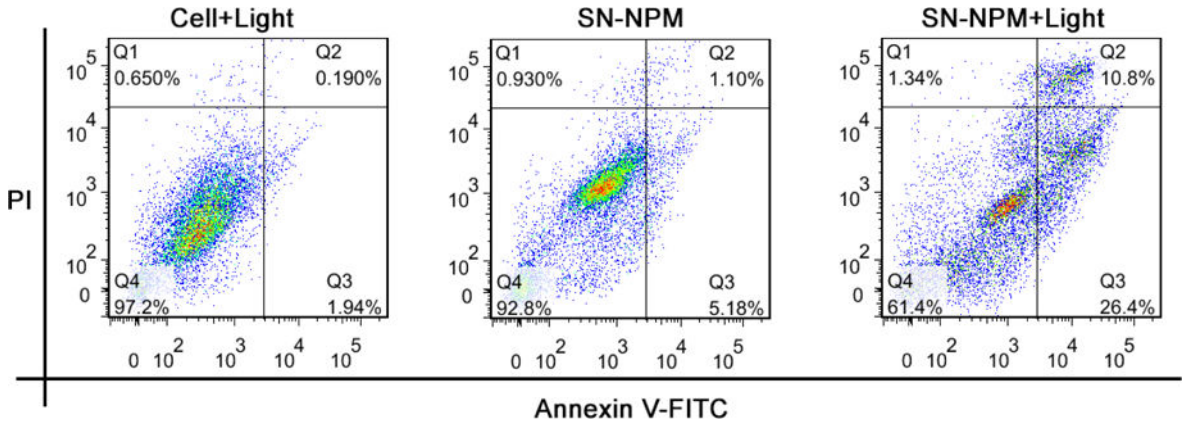

Fig. 5.

Apoptosis analysis on HT-29 colon cancer cells treated with SN-NPM with or without laser exposure.

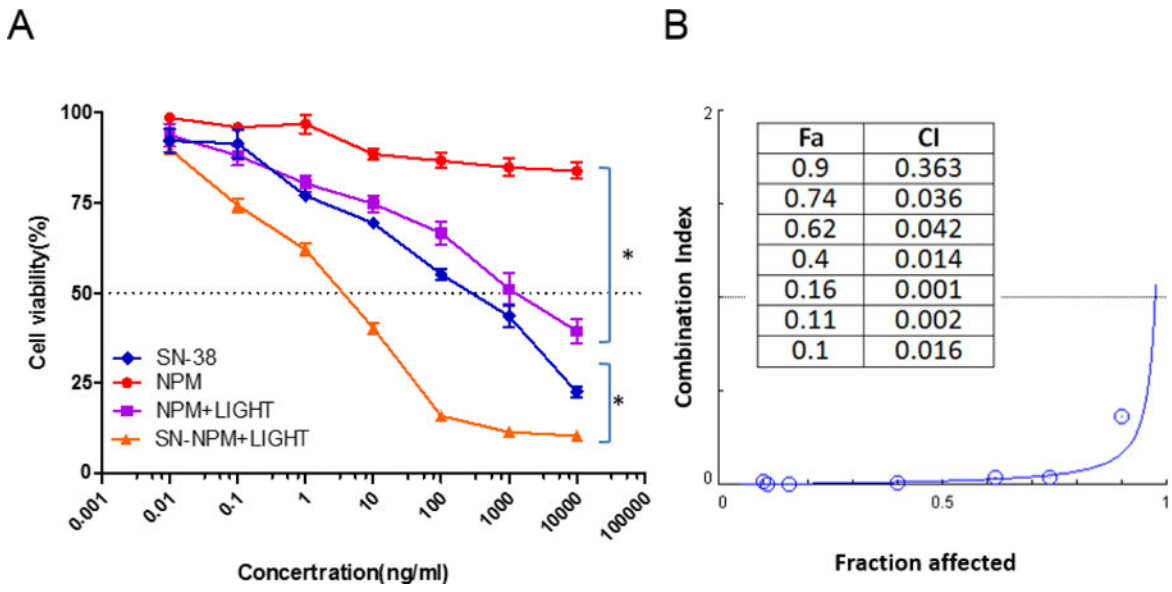

Fig. 6. The *in vitro* synergistic anti-cancer effects of SN-NPM mediated photo-chemotherapy

A) Cell viability changes upon SN-38, NPM, SN-NPM with or without light. The HT-29 human colon cancer cells were incubated with different concentrations of SN38, SN-NPM, and comparable amounts of NPM as SN-NPM for 24 hours. Cells were treated with LED panel light (635 nm) for 2 minutes, and cell viability was measured 72 hours later with MTS assay. (*$p<0.05$) B) Combination index (CI) versus Fraction affected (Fa) plot.

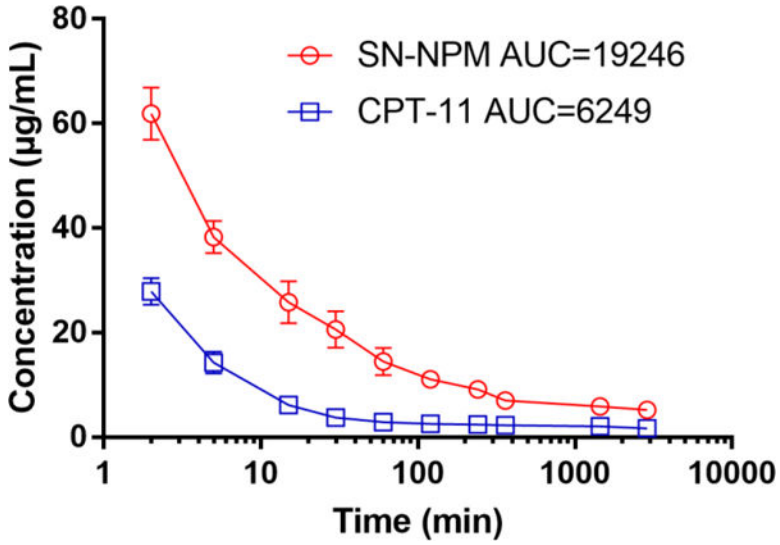

Fig. 7.

Pharmacokinetic profile of SN-NPM versus CPT-11 in rats. Blood were collected at different time points and serum was obtained to measure the fluorescence of SN-38 and CPT-11, respectively. The areas under the serum concentration curve (AUC) were calculated.

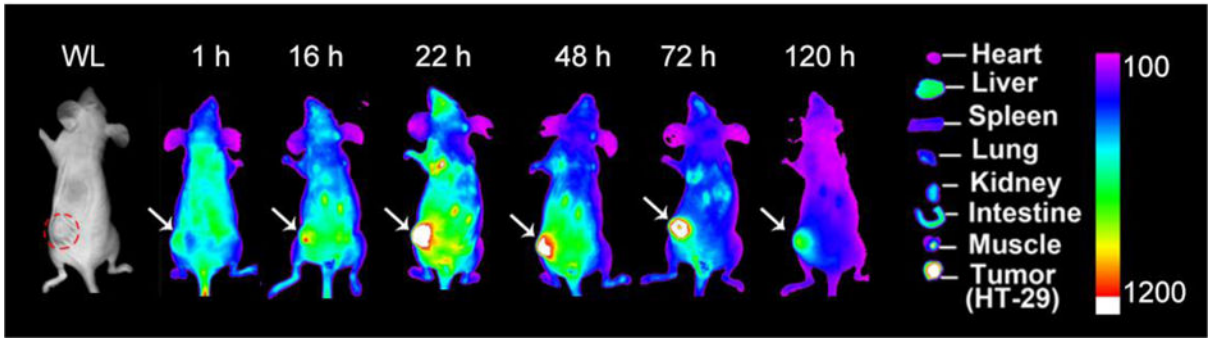

Fig. 8.

Biodistribution of SN-NPM in nude mice bearing HT-29 human colon cancer. Mice were given SN-NPM (NPM at 25 mg/kg) via tail vein and near-infrared fluorescence (NIRF) imaging was acquired at 1, 16, 22, 48, 72, and 120 hrs post-injection. (Right) *Ex vivo* NIRF imaging for tumors and major organs were performed at 22 hrs post-injection. WL, white light; Red circle and white arrows pointed out the position of tumor.

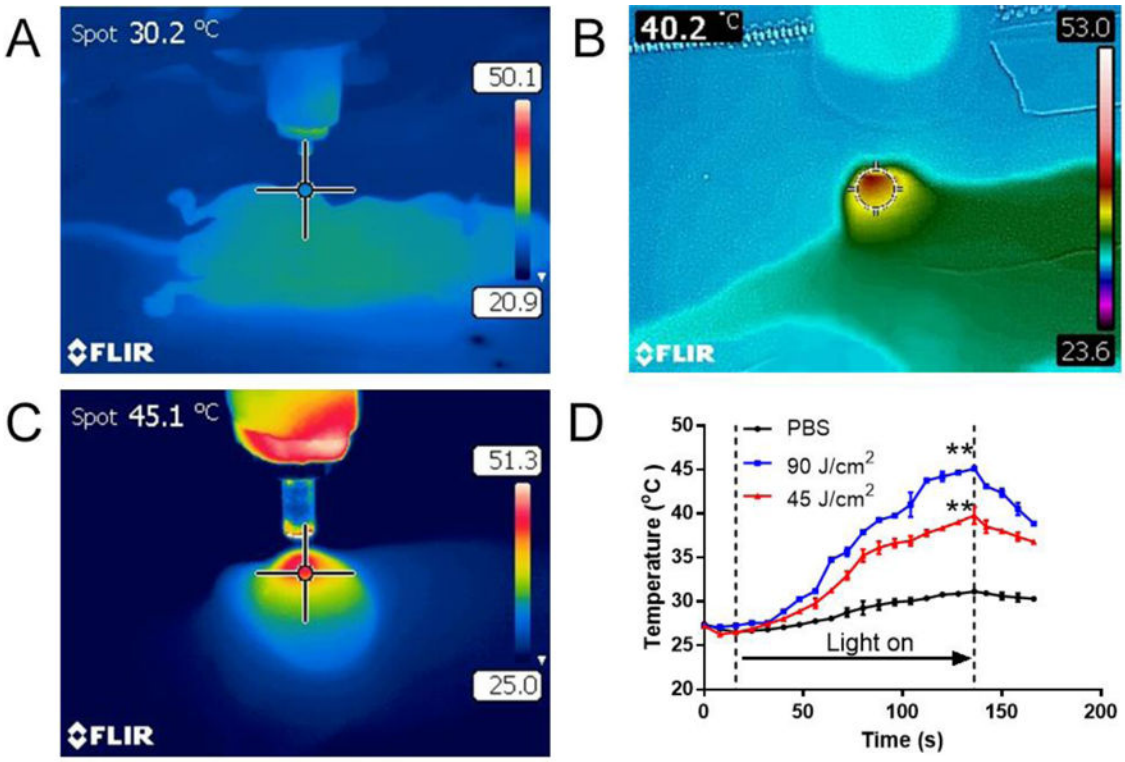

Fig. 9. SN-NPM mediated photothermal effect on nude mice bearing HT-29 human colon cancer

Representative thermal imaging of tumors treated by A) PBS, 90 J/cm^2, B) SN-NPM, 45 J/cm^2 and C) SN-NPM, 90 J/cm^2, the images were taken by the FLIR near-infrared camera. SN-NPM (25 mg/kg NPM) were injected via tail vein in the colon cancer bearing mice. Tumor sites were treated with 690 nm laser for two minutes after 24 hrs post-injection. The tumor temperature in the central spot was expressed at the left top corner. D) Temperature changes of tumors throughout the laser illumination in PBS (90 J/cm^2 laser), SN-NPM (45 J/cm^2 laser) and SN-NPM (90 J/cm^2 laser) pre-treated mice (**P<0.001, n=3).

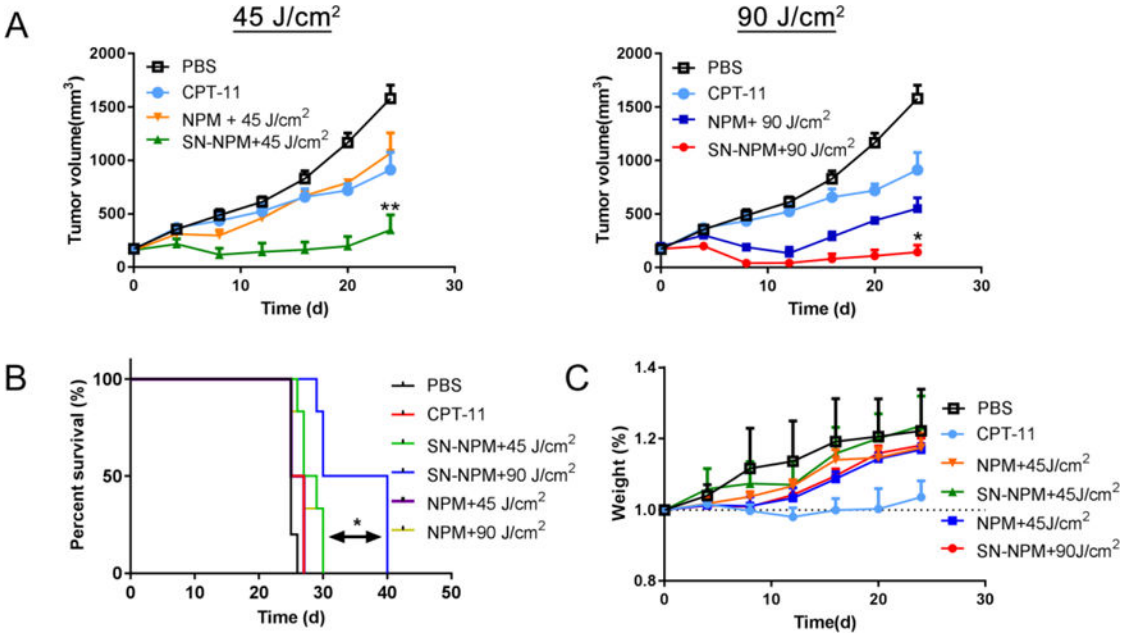

Fig. 10. The *in vivo* anti-tumor efficacy of SN-NPM against colon cancer in nude mice

PBS, CPT-11 (10 mg/kg), NPM, and SN-NPM (10 mg/kg) were i. v. injected on day 0, 4, and 8 in nude mice bearing HT-29 xenografts. Light treatments (690nm) were given on the tumors at 24 hrs post-injection. A). The tumor growth curve upon 45 J/cm^2 (left) and 90 J/cm^2 (right) laser light treatment (690nm). Of note, two Figs shared the same PBS and CPT-11 treated groups the treatment groups significantly inhibited the growth of tumor as compared with the controls **$p < 0.001$ (n=5). The survival curve B) and body weight changes C) for nude mice bearing colon cancer with the treatments as indicated. SN-NPM +90 J/cm^2 therapy led to significantly longer survival time. *$p<0.05$

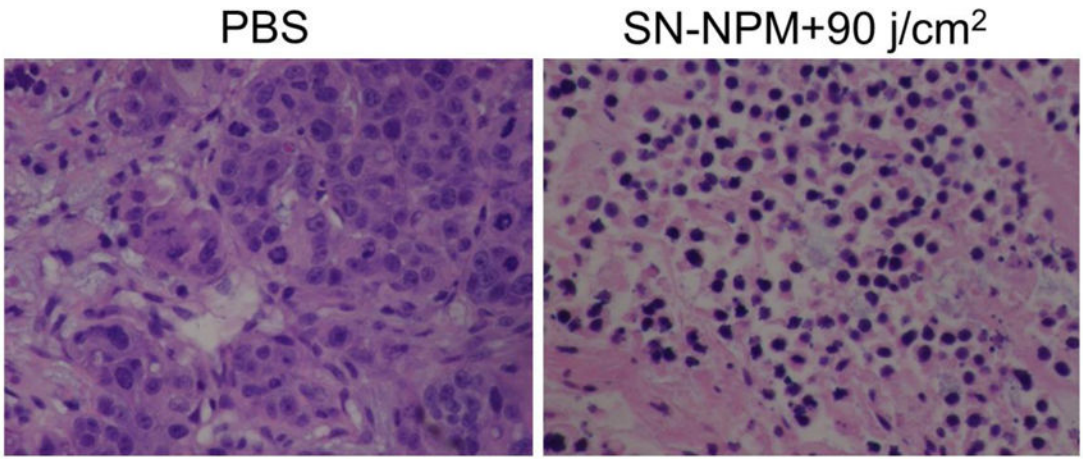

Fig. 11.

Microscopic evaluation of HT-29 xenograft after PBS and SN-NPM mediated tri-modality therapy (90 J/cm^2). (H&E, 40×)

Table 1

Drug loading, encapsulation efficiency, particle sizes and surface charges of SN-NPM.

D/T ratio[a]	Encapsulation Efficiency (%)[b]	Drug content (%)[c]	Mean size/nm (PDI)[d]	Zeta potential (mV)[d]
1/10	63.21±10.23	5.45	68.23±10.11 (0.412)	−7.34±0.55
1/20	85.12±6.53	4.05	23.21±8.23 (0.198)	−7.53±0.35
1/30	80.14±5.29	2.58	19.34±7.98 (0.201)	−7.77±0.17

[a] D/T ratio=weight of SN-38/weight of telodendrimer.

[b] Encapsulation efficiency (%)= [(Drug added - Free “unencapsulated drug”)/Drug added] *100

[c] Drug content (%)= [Encapsulated Drug/weight of whole nanoparticle] * 100

[d] Determined by dynamic light scattering (DLS)

Table 2

Summary of experimental design and tumor growth inhibition index for SN-NPM mediated tri-modality therapy on nude mice bearing HT-29 human colon cancer xenograft.

Treatment	CPT Dose (mg/kg)	Equivalent porphyrin dose (mg/kg)	Light total dose (J/cm^2)	%TGI[a]
Control	–	–	–	–
CPT-11	10	–	–	22.56
NPM +45 J/cm^2	–	17.9	45	28.36
SN-NPM +45 J/cm^2	10	17.9	45	71.96
NPM +90 J/cm^2	–	17.9	90	59.81
SN-NPM +90 J/cm^2	10	17.9	90	84.86*

*P<0.01, as compared with SN-NPM

[a]TGI (tumor growth inhibition) is presented as percent reduction in the mean tumor volume in experimental groups compared with saline-treated control groups.